Spectra and dynamics of quantum droplets in an optical lattice

Yuhang Nie,[1] Jun-Hui Zheng,[1,2,3,*] and Tao Yang[1,2,3,†]

[1]*Shaanxi Key Laboratory for Theoretical Physics Frontiers, Institute of Modern Physics, Northwest University, Xi'an 710127, China*

[2]*School of Physics, Northwest University, Xi'an 710127, China*

[3]*Peng Huanwu Center for Fundamental Theory, Xi'an 710127, China*

(Received 13 April 2023; revised 21 September 2023; accepted 24 October 2023; published 13 November 2023)

The optical lattice plays an important role in the stability and dynamics of quantum droplets. In this article, we investigate the Bogoliubov excitation spectrum of quantum droplets in an optical lattice in the thermodynamic limit. We classify the collective excitations as synchronous modes, Bloch phononic modes, and site-population-imbalanced modes. For synchronous modes, we measure the dipole oscillation frequencies by quench dynamics with a sudden shift of the optical lattice and the breathing frequencies by Floquet dynamics with a periodic change of the lattice depth. Bloch phononic modes are observable from the Landau critical velocity of the droplets. We further discuss the instability induced by site-dependent density fluctuations and calculate the critical filling of atoms where the growth of lattice vacancy breaks down the translational symmetry of the system. This work makes essential steps towards measuring the excitation spectrum and understanding the superfluid nature of quantum droplets in an optical lattice.

DOI: 10.1103/PhysRevA.108.053310

I. INTRODUCTION

Quantum droplets are self-bound states formed through a balance of particle-particle interactions without any external trapping, where attractions bring the constituent particles together and repulsions stabilize the droplets from collapse [1–14]. In experiments with ultracold atoms, quantum droplets have been achieved in single-component dipolar Bose-Einstein condensates (BECs) and binary BECs with interspecies attractions [15–21], where the competition arises from the mean-field interaction and the Lee-Huang-Yang (LHY) correction of the quantum zero-point energy [4,5,8–10]. The roles of these interactions in the formation of quantum droplets depend strongly on the dimensionality of the system [5]. It was shown that with a decreasing number of atoms N, free droplets become metastable and eventually disappear when N is smaller than a critical value. The excitations of free particle emissions, discrete monopole (breathing) modes, and surface ripplon modes of three-dimensional (3D) free droplets have also been well studied [4].

In systems with external traps, quantum droplets are stabilized further by suppression of the emission of free particles, and the trapping potential helps to manipulate the droplet mechanically [22,23]. The effect of a weak harmonic trapping potential on the surface modes of 3D quantum droplets was studied in Ref. [24]. However, the trapping confinements somehow obscure the characteristics of quantum droplets and become an obstacle to observing the formation and inflation of droplets. The optical lattice is an effective mean to stabilize droplets and their topography, which integrates not only the advantages of a trap but also the capability to show the growth of quantum droplets [25]. The existence of quantum droplets of bosonic mixtures in an optical lattice has been demonstrated in Ref. [26]. The formation of a quantum droplet of a two-component Bose gas in a two-dimensional (2D) optical lattice near the Mott insulator transition was studied in Ref. [27]. A variety of phases of droplets can be reached for bosonic atoms trapped in an optical lattice [28]. To understand the features of quantum droplets, accurate frequency measurement of collective modes is a powerful tool. For example, the collective mode measured in arrays of dipolar droplets clearly shows the symmetry breaking and the supersolid nature of the system [29,30]. Therefore, it is interesting to study the collective excitations of quantum droplets in optical lattices, which would be an excellent way to characterize this fascinating matter. It is also helpful to probe the interplay between light and condensed matter, which usually brings novel phenomena [31–38].

It is crucial to study 2D quantum droplets theoretically due to the fact that the quantum effects strongly depend on dimensionality. Weakly interacting low-dimensional Bose-Bose mixtures present themselves as promising candidates for investigating liquid phases in the ultracold ultradilute regime and studying associated beyond-mean-field effects. In the one-dimensional (1D) case, the droplet phase is formed when the effective mean-field interaction is repulsive and the interaction from the LHY correction is attractive [5], contrasting the 3D case where a positive LHY correction is required to stabilize the mixture with effective attractive interaction [4]. The behavior in the 2D case exhibits a more intricate nature. It has been shown that the resulting states induced by dragging a defect in droplet BECs with different dimensions are different [39]. Even though there are still some challenges in realizing the corresponding 2D quantum droplets in binary

*junhui.zheng@nwu.edu.cn
†yangt@nwu.edu.cn

BECs [40], recent experimental efforts have been directed towards 2D quantum droplets [41–43].

In this article, we consider an infinitely large system of 2D quantum droplets in an optical lattice. Therefore, the boundary effects of a cluster of lattice quantum droplets existing in a finite-size system are negligible and one can focus on the universal behaviors of droplets. In Secs. II and III, the ground state and the Bogoliubov excitation spectrum of the quantum droplets for different lattice depths are calculated by using the imaginary time evolution method and the exact diagonalization method, respectively. Bloch phononic modes are observable from the Landau critical velocity of the droplets by exciting density waves [44,45]. The properties of quench dynamics and Floquet dynamics of the droplets are investigated by suddenly shifting the lattice potential and periodically driving the system [46,47]. The oscillation frequency and intrinsic breathing frequency obtained agree very well with the Bogoliubov excitation spectrum and are measurable in ongoing experiments. Moreover, as shown in Sec. IV, number imbalances among different sites of the lattice may induce instability of the droplets. We find that below a critical filling, vacancies in the lattice appear spontaneously, and the translational symmetry of the system breaks down, which is the prelude to producing the self-assembly of quantum droplets from different sites.

II. DESCRIPTION OF LATTICE DROPLETS

Considering a binary BEC loaded in a 2D optical lattice and taking into account the Lee-Huang-Yang correction, the two components of the BEC with the same scattering length and particle number can be described by a common wave function. This wave function, in a rescaled form, follows the extended Gross-Pitaevskii equation (GPE) in the dimensionless form [25,48]

$$i\partial_t\phi = -\tfrac{1}{2}\nabla^2\phi + V(x,y)\phi + |\phi|^2\phi\ln|\phi|^2, \tag{1}$$

where the 2D optical lattice potential reads

$$V(x,y) = V_0\left[\sin^2\left[\pi\left(\frac{x}{d}+\delta\right)\right] + \sin^2\left(\frac{\pi}{d}y\right)\right]. \tag{2}$$

Here, V_0 is the optical lattice depth, d is the lattice constant, and δ is used to shift the entire lattice.

The growth of quantum droplets in lattices was analyzed in Ref. [25]. Since the density profiles at each occupied lattice site are almost the same and we focus on excitation modes of lattice quantum droplets, we consider the thermodynamic limit that all lattice sites are occupied by droplets (i.e., the system preserves translational symmetry) and control the particle number per lattice site (i.e., the filling of the system)

$$N_s = \iint_{d^2} |\phi|^2 dxdy. \tag{3}$$

The energy per site is

$$E_s = \frac{1}{2}\iint_{d^2}\left[|\nabla\phi|^2 + 2V|\phi|^2 + |\phi|^4\ln\left(\frac{|\phi|^2}{\sqrt{e}}\right)\right]dxdy. \tag{4}$$

In the absence of the external potential V, the density distribution of a quantum droplet is flat everywhere except at boundaries for a sufficiently large total particle number N. After neglecting the surface energy (i.e., taking into account uniform distribution), minimizing the total energy $E \simeq (N/2)\rho\ln(\rho/\sqrt{e})$ gives the favored density $\rho_0 = \exp(-1/2) \simeq 0.61$ [5]. Note that the condition of minimizing the total energy (at zero temperature) is equivalent to requiring vanishing pressure $p = -\partial E/\partial A|_N = (\rho^2/N)\partial E/\partial\rho|_N = 0$, where $A = N/\rho$ is the area of the droplet [5,49]. In an optical lattice, the ground-state wave function ϕ_0 can be obtained by numerically solving Eq. (1) in the imaginary time evolution using the Crank-Nicholson method [50]. We use an initial state $\phi = \sqrt{N_s}/d^2$ in each cell for simplicity, without affecting the final results. We discretize the unit cell of the optical lattice into 80×80 grids and use the imaginary time spacing of 0.005. For wave functions $\zeta \propto \xi \doteq -\frac{1}{2}\nabla^2\phi + V(x,y)\phi + |\phi|^2\phi\ln|\phi|^2$ with ζ being normalized to N_s, we obtain the final self-consistent ground-state wave function with good precision: $\langle\zeta|\phi\rangle/N_s \geqslant 1 - 10^{-6}$. The chemical potential μ is determined by $\mu = \sqrt{\langle\xi|\xi\rangle/N_s}$. We note that the low-energy part of the Bogoliubov spectrum are highly sensitive to the precision of the ground-state wave function, and thus high accuracy is required.

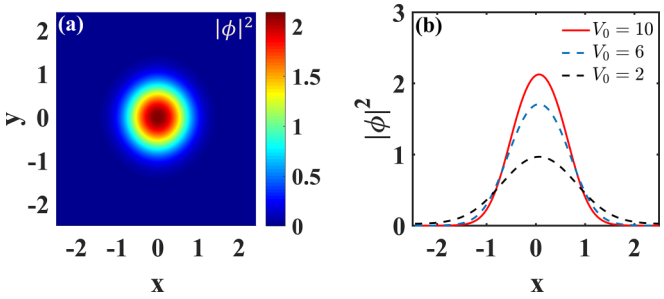

FIG. 1. Density distribution of quantum droplets in one cell of an optical lattice with filling $N_s = 3.5$. (a) The top view of the density distribution for $V_0 = 10$. (b) The cross sections of the density distribution at $y = 0$ for $V_0 = 2$, 6, 10, respectively.

In Fig. 1(a), we show the density profile of the ground-state quantum droplet in a single unit cell for $V_0 = 10$, $d = 5$, and $N_s = 3.5$. The droplets at different sites are the same in both size and shape. The existence of the optical lattice significantly changes the flat-top structure of the density profile (the near-flat-top structure can be recovered for shallow lattices with a large value of d and a small value of V_0 such that the change of potential in the scale of the healing length ξ is small, i.e., $V_0\xi/d \ll |\rho_0\ln\rho_0|$). With increasing depth of the lattice, the peak density increases accordingly, while the radius of the droplet decreases, as shown in Fig. 1(b). The peak densities of the droplets in the lattice are all higher than ρ_0 to minimize the energy of the system. From Eq. (1), we see that the effective potential contributed by atom-atom interaction is negative for $\rho < 1$ and positive for $\rho > 1$. Thus, with decreasing V_0, the system may undergo a transition from effectively repulsive interactions to attractive interactions when the peak density becomes smaller than 1. For cases with large V_0, the central part of the droplet is dominated by the repulsive interaction, while the attractive interaction dominates the rim of the droplet at each site.

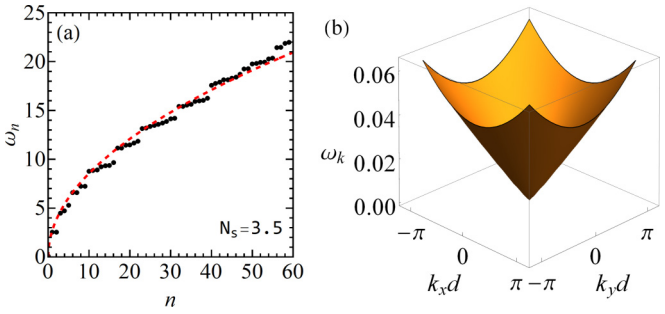

FIG. 2. Bogoliubov spectrum of collective excitations of lattice quantum droplets for $V_0 = 10$. (a) The synchronous excitation modes. The dashed red line is the fitting function $n = \alpha\omega^2$ with a parameter α. (b) The Bloch phononic spectra.

In the next section, we calculate the excitation spectra of lattice droplets. Since the methods applied to detect the spectra do not depend on the parameter set, in the following, we set $d = 5$ as an example. Similar discussions can be extended to general cases. The sign of effective potential can be tuned by changing the filling factor N_s and the lattice depth V_0.

III. BOGOLIUBOV SPECTRA AND DYNAMICS STUDY

The collective excitation modes can be obtained by considering a small fluctuation around the ground-state wave function $\phi_0(x, y, t) = \psi_0(x, y)e^{-i\mu t}$, i.e., $\phi = (\psi_0 + \psi_1)e^{-i\mu t}$. By expanding Eq. (1) with respect to ψ_1 and ψ_1^*, we obtain the evolution equation of the fluctuation ψ_1 under the linear approximation

$$i\partial_t\psi_1 = -\tfrac{1}{2}\nabla^2\psi_1 + V\psi_1 + \left(2\psi_0^2\psi_1 + \psi_0^2\psi_1^*\right)\ln\psi_0^2 + \psi_0^2(\psi_1 + \psi_1^*) - \mu\psi_1, \tag{5}$$

and its conjugate equation. Now, we consider the excitation mode $\psi_1 = \tilde{u}e^{-i\omega t} + \tilde{v}^*e^{i\omega t}$, and assume that the wave function takes the form of the Bloch wave, i.e., $\tilde{u}(\boldsymbol{r}) = e^{i\boldsymbol{k}\cdot\boldsymbol{r}}u_{\boldsymbol{k}}(\boldsymbol{r})$ and $\tilde{v}(\boldsymbol{r}) = e^{i\boldsymbol{k}\cdot\boldsymbol{r}}v_{\boldsymbol{k}}(\boldsymbol{r})$, where both $u_{\boldsymbol{k}}(\boldsymbol{r})$ and $u_{\boldsymbol{k}}(\boldsymbol{r})$ are periodic in space, similar to the ground state and the lattice potential. As a result, we obtain

$$\omega_{\boldsymbol{k}}\begin{pmatrix} u_{\boldsymbol{k}} \\ v_{\boldsymbol{k}} \end{pmatrix} = \begin{pmatrix} A & B \\ -B & -A \end{pmatrix}\begin{pmatrix} u_{\boldsymbol{k}} \\ v_{\boldsymbol{k}} \end{pmatrix}, \tag{6}$$

where

$$A = \tfrac{1}{2}\boldsymbol{k}^2 - i\boldsymbol{k}\cdot\nabla - \tfrac{1}{2}\nabla^2 + V + 2\psi_0^2\ln\psi_0^2 + \psi_0^2 - \mu, \tag{7}$$

$$B = \psi_0^2\ln\psi_0^2 + \psi_0^2. \tag{8}$$

By discretizing real space and using the obtained ground-state wave function ψ_0 and the chemical potential μ from the previous calculation, we numerically calculate the Bogoliubov spectrum of the collective excitations by performing an exact diagonalization of the matrix $\left(\begin{smallmatrix} A & B \\ -B & -A \end{smallmatrix}\right)$ for the given $k_x, k_y \in [-\pi/d, \pi/d]$. In Fig. 2(a), we show the excitation spectrum for the given $\boldsymbol{k} = 0$. In this case, the wave functions of the excited states possess translational invariance, which can be named as synchronous excitation modes of the quantum droplets in the lattice. For large V_0, we can find that the total number of states below energy ω approximately satisfies $n \sim \alpha\omega^2$ with α being a fitting parameter. This result is similar to that of the number of states of a noninteracting system in a harmonic trap. For a noninteracting bose gas in a harmonic trap with $\omega_h = \sqrt{2V_0}\pi/d$, the spectra are $\omega_{n_r l} = (2n_r + |l|)\omega_h$, and the total number of states below energy ω is $n \sim \omega^2/2\omega_h^2$, where n_r is the radial quantum number and l is the angular momentum quantum number. For a deep lattice, each site can be approximated as a harmonic trap. Thus, the fitting parameter α depends on the values of ω_h and N_s, the latter of which influences the properties of the interaction. For $N_s = 3.5$ and $V_0 = 10$, we note that this fitting is still valid for the excitation spectrum up to $n = 60$. But for excitations with higher energy or a shallow lattice, the ω_n-n relation deviates significantly from the fitting function.

From the energy spectrum Fig. 2(a), we can clearly see that the first excitation is double degenerate, which is due to the C_4 symmetry of the optical lattice in the x-y plane. These two excitations correspond to the excitation modes $(n_r, l) = (0, \pm 1)$ of a harmonically trapped noninteracting system, and the next three excitations correspond to the degenerate excitation modes $(n_r, l) = (1, 0), (0, \pm 2)$. With repulsive interaction, in a harmonic trap, the spectrum becomes $\omega_{n_r l} = \omega_h\sqrt{2n_r + 2n_r^2 + 2n_r|l| + |l|}$ where the breathing mode (1,0) and the other two are not degenerate [51]. In addition, the U(1) rotational symmetry of a harmonic trap is broken for a lattice, which will lead to further splitting of the rest two modes. In Fig. 2(b), we plot the phononic spectra of the Bloch waves in the first Brillouin zone. In experiments, it is convenient to determine phononic excitation spectra by measuring the Landau critical velocity of the superfluid [44,45]. This velocity ($\simeq 0.073$) is the gradient of the dispersion relation along different directions at $\boldsymbol{k} = 0$. In contrast to the synchronous excitation modes, the Bloch waves focus on the phase fluctuation of the system: the density distributions in different lattices remain the same but the phases vary. We also find that the group velocities of phononic excitations along different directions are almost the same. All the spectra shown in Figs. 2(a) and 2(b) are real and positive, indicating that the system is stable under synchronous excitations or phase fluctuations.

The synchronous excitation spectrum can be obtained from the dynamics of the droplets. In the following, we will study the quench dynamics and Floquet dynamics of the droplet in the lattice. By suddenly shifting the lattice for 5% of the lattice constant along the x (y) direction, we identify the oscillation mode of the droplets under quench dynamics. As a result, the center of mass of the droplets $\bar{x} = \int_{\text{cell}}(x + d\delta)\rho(\boldsymbol{r})d\boldsymbol{r}$ deviate from the minimum of each cell of the lattice potential. The droplets start to oscillate in the x (y) direction. The typical oscillating behavior of the center of mass ($\bar{x}$) of the droplet is $\cos(\Omega_1 t)$ as shown in Fig. 3(a). The magnitude of Ω_1 can be obtained by fitting the evolution of the oscillation.

By periodically modulating the potential depth with

$$V_0 \to V_0 + \delta V\sin(\nu t), \tag{9}$$

we can identify the breathing mode of the droplets under Floquet dynamics. The density of particles ρ_c at the center of each cell of the lattice varies with the potential depth, which can be employed to characterize the breathing behavior. For different initial potential depths V_0, we set the modulation amplitude to be $\delta V = 5\%V_0$ and tune the driving frequency

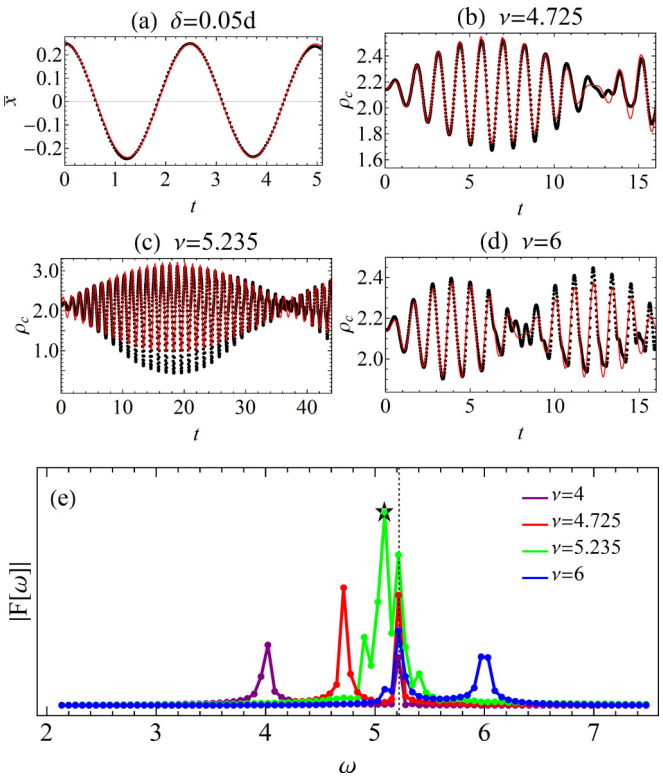

FIG. 3. (a) The center of mass of the droplet changes over time during quench dynamics when the lattice is suddenly shifted. The dotted line is the numerical result. The red solid line is the fitting result with the cosine function $\cos(\Omega_1 t)$. (b)–(d) The evolution of the density (ρ_c) at the center of each site for different driving frequencies ν. The dotted lines are numerical results. The red solid lines show the fitting results of $a_0 + a_1 \sin(\nu t) + a_2 \sin(\omega t)$, where ω equals the breathing frequency ($\omega_n = 5.235$) for (b) and (d), but is shifted to $\tilde{\omega} \simeq 5.06$ for the resonant case (c). (e) The spectrum function obtained from the Fourier transformation of $\rho_c(t)$ over the interval $t \in [0, 100]$ for different driving frequencies ν. Both the driving frequency and intrinsic frequency are reflected in the corresponding spectrum function.

ν. For $V_0 = 10$ as shown in Figs. 3(b) to 3(d), the time evolutions of ρ_c exhibit regular oscillating behaviors with different amplitudes and periods by applying three typical driving frequencies. When the amplitude is sufficiently large, it becomes asymmetric [see Fig. 3(c)] due to nonlinear effects.

We further apply the Fourier transform to obtain the spectrum functions of the above oscillations with $t \in [0, 100]$. As shown in Fig. 3(e), we observe that when the driven frequency is away from the spectrum of the "second" synchronous excitation (the "first" synchronous excitation is the oscillation excitation), there are two frequencies that dominate the spectrum function. One frequency is nothing but the driven frequency itself and the other one remains unchanged when tuning ν. Therefore, we match this intrinsic frequency Ω_2 ($\simeq$ 5.22, see the black dashed line) to the frequency of the breathing mode ($\omega_n = 5.235$) of the droplets. Basically, the closer the driving frequency is to Ω_2, the greater the oscillation amplitude and the longer the period [see Figs. 3(b) to 3(d)]. The fitting function $a_0 + a_1 \sin(\nu t) + a_2 \sin(\omega_n t)$ agrees very well with the real-time evolution $\rho_c(t)$, as shown in Figs. 3(b) and 3(d). However, in the near-resonant regime ($\nu - \Omega_2 \ll \Omega_2$), the spectrum function indicated by the green solid line ($\nu = 5.235$) in Fig. 3(e) gives more structures around Ω_2, and the obtained frequency ($\simeq 5.086$, marked by a black star) besides the driven frequency, deviates slightly from the intrinsic frequency. Fitting $\rho_c(t)$ with $a_0 + a_1 \sin(\nu t) + a_2 \sin(\tilde{\omega} t)$ gives $\tilde{\omega} \simeq 5.06$ and the resulting function is shown in Fig. 3(c). Near the resonance region, we describe the dynamical system using a two-level model

$$H_{2-\text{level}} = \begin{pmatrix} \Omega_2 & \Delta \sin(\nu t) \\ \Delta \sin(\nu t) & 0 \end{pmatrix}. \tag{10}$$

The rotating wave approximation gives the new spectrum with the reference frequency ν,

$$\frac{\Omega_2 - \nu}{2} \pm \sqrt{\frac{(\Omega_2 - \nu)^2}{4} + \frac{\Delta^2}{4}}, \tag{11}$$

which introduces energy split $\pm\Delta/2$ when ν coincides with Ω_2. Therefore, we attribute the emergence of $\tilde{\omega}$ to the hybridization effect of the driving and resonating frequencies.

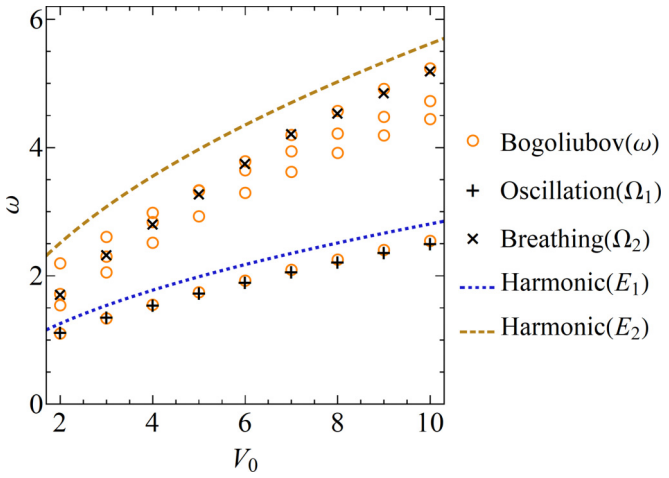

FIG. 4. The Bogoliubov spectra (orange circles), the dynamical dipole oscillation frequencies (black "+"), the intrinsic breathing frequencies (black "×"), and the excitation spectra (dashed lines, $E_2 = 2E_1 = 2\omega_h$) in the harmonic trap with frequency $\omega_h = \sqrt{2V_0}\pi/d$.

In Fig. 4, we plot the oscillating frequency Ω_1 (marked by black "+"), the intrinsic frequency Ω_2 (marked by black "×"), and the Bogoliubov spectrum of synchronous excitations (marked by orange circles) with respect to the lattice depth V_0. We can see that Ω_1 fits the Bogoliubov spectrum very well and Ω_2 is located in one of the three "second" synchronous excitation modes that corresponds to the breathing mode and is about twice that of Ω_1 for $V_0 \geqslant 5$ but significantly less than twice of Ω_1 in a shallow lattice where attractive interaction dominates. The dashed solid lines refer to the oscillating excitation in a harmonic trap with frequency ω_h. This harmonic trap is the second-order approximation of the lattice potential whose first excitation (dipole oscillation) is $E_1 = \omega_h$ with two degenerate modes, while the breathing excitation is $E_2 = 2\omega_h$ for cases with repulsive interaction or without interaction. The Bogoliubov spectrum is generally smaller than that in the harmonic trap, as the confinement effect from the lattice potential is weaker.

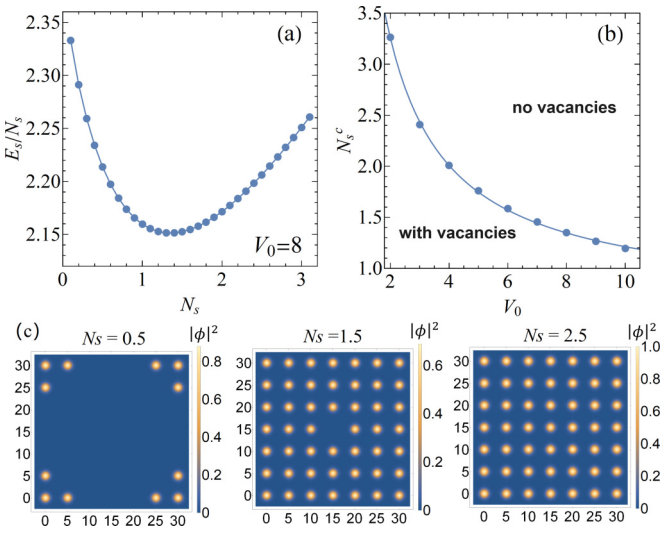

FIG. 5. (a) The energy per atom E_s/N_s varying with the filling N_s. (b) The critical filling as a function of lattice depth V_0. The solid line is the fitting result of $b_0 + b_1/(V_0 + b_2)$ with $b_0 = 0.661$, $b_1 = 5.59$, and $b_2 = 0.156$. (c) The appearance of vacancies in lattice quantum droplets for $V_0 = 3$ with low fillings.

IV. SPONTANEOUS EMERGENCE OF VACANCIES

In our calculations above, we assumed that the density distribution of the droplet at each lattice site remains the same. Therefore, the population imbalance between different lattice sites is completely ignored. For cases with a large filling, the repulsive interaction dominates, and thus the imbalance is strongly suppressed. The validity of the equal population assumption at different sites is guaranteed. However, in cases with low filling, the attractive interaction becomes stronger. In this situation, small density fluctuations may induce the emergence of self-binding, leading to the appearance of vacancies in the lattice or even the formation of clusters of quantum droplets from different sites.

Note that when vacancies start to appear in some sites of the lattice, the filling of particles in other sites will increase to keep the total number of particles constant. Here, we introduce the single-atom energy, $\varepsilon \doteq E_s/N_s$ [5]. If ε decreases with increasing N_s, it means that the system with vacancies has lower energy. Therefore, the translational symmetry of the system will break down. Otherwise, the system with an even population in all sites is stable. In Fig. 5(a), we plot the single-atom energy ε as a function of the filling N_s for different lattice depths V_0. The figure shows that ε decreases first and then increases as N_s increases. The turning point is the critical filling for the phase transition. In Fig. 5(b), we plot the critical filling as a function of lattice depth V_0. With increasing V_0, the critical filling decreases approximately with $b_0 + b_1/(V_0 + b_2)$, where $b_0 = 0.661$, $b_1 = 5.59$, and $b_2 = 0.156$. This is because with the same filling, the density is smaller and the attractive interaction is stronger in a shallow lattice potential. As an example, we consider a 7×7 lattice ($d = 5$) with periodic boundary conditions and introduce a small defect (a Gaussian potential with $\Delta V = 0.01 \exp[-(x^2 + y^2)/8]$, which is used to fix the position of the vacancy when it appears) in the potential at the center of the lattice. We use 560×560 grids in the numerical simulation. As shown in Fig. 5(c), we observe the appearance of vacancies with a decrease in the averaged N_s per site. For $N_s = 0.5$, since the appearance of vacancy, the average filling for the filled sites becomes $0.5 \times 49/12 \simeq 2.04$, which is significantly greater than N_s.

V. CONCLUSION

In conclusion, optical lattices provide a powerful tool for investigating model systems of quantum droplets in periodic potentials through probing excitation properties and nonlinear dynamics. Here, we investigated the excitation spectrum, quench dynamics, and Floquet dynamics, and the stability of quantum droplets in an optical lattice in the thermodynamic limit. We find different excitation modes, including the synchronous excitations of droplets from different lattice sites, the Bloch phononic excitation from phase fluctuations, and excitations from site-dependent density fluctuations. Both dipole oscillations and breathing modes belong to synchronous excitations. By directly fitting the center of mass and the density variation of the droplets, or by spectrum analysis through Fourier transformation, we show that the dynamics faithfully record the frequencies of dipolar oscillations and breathing modes. This provides reliable means to detect the excitation spectra in experiments [46,47]. In addition, the measurement of the Landau critical velocity of the superfluid can be used to determine the group velocity of the Bloch phonons [44,45]. These results are measurable when the 2D lattice quantum droplets are prepared. Moreover, when considering the site-dependent density fluctuations, the system with low fillings may become unstable, leading to the formation of vacancies in certain sites of the optical lattice. This process breaks the translational symmetry and is the precursor to the formation of clusters of lattice quantum droplets, which result from the combination of density fluctuations and effective attractive interactions. With the possible emergence of an array of vacancies, our system is a very good candidate for probing a new supersolid phase [52,53].

ACKNOWLEDGMENTS

This work is supported by the National Natural Science Foundation of China under Grants No. 12175180, No. 11934015, and No. 12247103, the Major Basic Research Program of Natural Science of Shaanxi Province under Grants No. 2017KCT-12 and No. 2017ZDJC-32, and Shaanxi Fundamental Science Research Project for Mathematics and Physics under Grants No. 22JSZ005 and No. 22JSQ041. This research is also supported by The Double First-Class University Construction Project of Northwest University.

[1] M. Bender, P. H. Heenen, and P. G. Reinhard, Self-consistent mean-field models for nuclear structure, Rev. Mod. Phys. **75**, 121 (2003).

[2] F. Dalfovo and S. Stringari, Helium nanodroplets and trapped Bose–Einstein condensates as prototypes of finite quantum fluids, J. Chem. Phys. **115**, 10078 (2001).

[3] A. Bulgac, Dilute quantum droplets, Phys. Rev. Lett. **89**, 050402 (2002).

[4] D. S. Petrov, Quantum mechanical stabilization of a collapsing Bose-Bose mixture, Phys. Rev. Lett. **115**, 155302 (2015).

[5] D. S. Petrov and G. E. Astrakharchik, Ultradilute low-dimensional liquids, Phys. Rev. Lett. **117**, 100401 (2016).

[6] C. Staudinger, F. Mazzanti, and R. E. Zillich, Self-bound Bose mixtures, Phys. Rev. A **98**, 023633 (2018).

[7] Y. Sekino and Y. Nishida, Quantum droplet of one-dimensional bosons with a three-body attraction, Phys. Rev. A **97**, 011602(R) (2018).

[8] D. Baillie, R. M. Wilson, R. N. Bisset, and P. B. Blakie, Self-bound dipolar droplet: a localized matter wave in free space, Phys. Rev. A **94**, 021602(R) (2016).

[9] L. Chomaz, S. Baier, D. Petter, M. J. Mark, F. Wachtler, L. Santos, and F. Ferlaino, Quantum-fluctuation-driven crossover from a dilute Bose-Einstein condensate to a macrodroplet in a dipolar quantum fluid, Phys. Rev. X **6**, 041039 (2016).

[10] F. Wächtler and L. Santos, Ground-state properties and elementary excitations of quantum droplets in dipolar Bose–Einstein condensates, Phys. Rev. A **94**, 043618 (2016).

[11] P. Zin, M. Pylak, T. Wasak, M. Gajda, and Z. Idziaszek, Quantum Bose-Bose droplets at a dimensional crossover, Phys. Rev. A **98**, 051603(R) (2018).

[12] T. Ilg, J. Kumlin, L. Santos, D. S. Petrov, and H. P. Büchler, Dimensional crossover for the beyond-mean-field correction in Bose gases, Phys. Rev. A **98**, 051604(R) (2018).

[13] Z.-H. Luo, W. Pang, B. Liu, Y.-Y. Li, and B. A. Malomed, A new form of liquid matter: Quantum droplets, Front. Phys. **16**, 32201 (2021).

[14] Y. Li, Z. Luo, Y. Liu *et al.*, Two-dimensional solitons and quantum droplets supported by competing self- and cross-interactions in spin-orbit-coupled condensates, New J. Phys. **19**, 113043 (2017).

[15] M. Schmitt, M. Wenzel, F. Bttcher, I. Ferrier-Barbut, and T. Pfau, Self-bound droplets of a dilute magnetic quantum liquid, Nature (London) **539**, 259 (2016).

[16] C. R. Cabrera L. Tanzi, J. Sanz *et al.*, Quantum liquid droplets in a mixture of Bose-Einstein condensates, Science **359**, 301 (2017).

[17] P. Cheiney, C. R. Cabrera, J. Sanz, B. Naylor, L. Tanzi, and L. Tarruell, Bright soliton to quantum droplet transition in a mixture of Bose-Einstein condensates, Phys. Rev. Lett. **120**, 135301 (2018).

[18] I. Ferrier-Barbut, H. Kadau, M. Schmitt, M. Wenzel, and T. Pfau, Observation of quantum droplets in a strongly dipolar Bose gas, Phys. Rev. Lett. **116**, 215301 (2016).

[19] H. Kadau, M. Schmitt, M. Wenzel *et al.*, Observing the Rosensweig instability of a quantum ferrofluid, Nature (London) **530**, 194 (2016).

[20] G. Semeghini, G. Ferioli, L. Masi *et al.*, Self-bound quantum droplets of atomic mixtures in free space, Phys. Rev. Lett. **120**, 235301 (2018).

[21] I. Ferrier-Barbut, M. Wenzel, F. Böttcher, T. Langen, M. Isoard, S. Stringari, and T. Pfau, Scissors mode of dipolar quantum droplets of dysprosium atoms, Phys. Rev. Lett. **120**, 160402 (2018).

[22] L. Dong and Y. V. Kartashov, Rotating multidimensional quantum droplets, Phys. Rev. Lett. **126**, 244101 (2021).

[23] M. N. Tengstrand, P. Stürmer, E. Ö. Karabulut, and S. M. Reimann, Rotating binary Bose-Einstein condensates and vortex clusters in quantum droplets, Phys. Rev. Lett. **123**, 160405 (2019).

[24] H. Hu and X.-J. Liu, Collective excitations of a spherical ultradilute quantum droplet, Phys. Rev. A **102**, 053303 (2020).

[25] Y.-Y. Zheng, S.-T. Chen, Z.-P. Huang, S.-X. Dai, B. Liu, Y.-Y. Li, and S.-R. Wang, Quantum droplets in two-dimensional optical lattices, Front. Phys. **16**, 22501 (2021).

[26] I. Morera, G. E. Astrakharchik, A. Polls, and B. Juliá-Díaz, Quantum droplets of bosonic mixtures in a one-dimensional optical lattice, Phys. Rev. Res. **2**, 022008(R) (2020).

[27] Y. Machida, I. Danshita, D. Yamamoto, and K. Kasamatsu, Quantum droplet of a two-component Bose gas in an optical lattice near the Mott insulator transition, Phys. Rev. A **105**, L031301 (2022).

[28] P. Karpov and F. Piazza, Light-induced quantum droplet phases of lattice bosons in multimode cavities, Phys. Rev. Lett. **128**, 103201 (2022).

[29] L. Tanzi, S. M. Roccuzzo, E. Lucioni *et al.*, Supersolid symmetry breaking from compressional oscillations in a dipolar quantum gas, Nature (London) **574**, 382 (2019).

[30] M. Guo, F. Böttcher, J. Hertkorn *et al.*, The low-energy Goldstone mode in a trapped dipolar supersolid, Nature (London) **574**, 386 (2019).

[31] O. Morsch and M. Oberthaler, Dynamics of Bose-Einstein condensates in optical lattices, Rev. Mod. Phys. **78**, 179 (2006).

[32] H. Chen, Y. Liu, Q. Zhang, Y. Shi, W. Pang, and Y. Li, Dipolar matter-wave solitons in two-dimensional anisotropic discrete lattices, Phys. Rev. A **93**, 053608 (2016).

[33] R. Zaera, J. Vila, J. Fernandez-Saez, and M. Ruzzene, Propagation of solitons in a two-dimensional nonlinear square lattice, Int. J. Non Linear Mech. **106**, 188 (2018).

[34] Z. Zhou, X. Yu, Y. Zou, and H. Zhong, Dynamics of quantum droplets in a one-dimensional optical lattice, Commun. Nonlinear Sci. Numer. Simul. **78**, 104881 (2019).

[35] L. Dong, W. Qi, P. Peng, L. Wang, H. Zhou, and C. Huang, Multi-stable quantum droplets in optical lattices, Nonlinear Dyn. **102**, 303 (2020).

[36] J. Chen and J. Zeng, One-dimensional quantum droplets under space-periodic nonlinear management, Results Phys. **21**, 103781 (2021).

[37] F.-Y. Zhao, Z.-T. Yan, X.-Y. Cai, C.-L. Li, G.-L. Chen, H.-X. He, B. Liu, and Y.-Y. Li, Discrete quantum droplets in one-dimensional optical lattices, Chaos, Solitons & Fractals **152**, 111313 (2021).

[38] X. Zhang, X. Xu, Y. Zheng, Z. Chen, B. Liu, C. Huang, B. A. Malomed, and Y. Li, Semidiscrete quantum droplets and vortices, Phys. Rev. Lett. **123**, 133901 (2019).

[39] S. Saqlain, T. Mithun, R. Carretero-González, and P. G. Kevrekidis, Dragging a defect in a droplet Bose-Einstein condensate, Phys. Rev. A **107**, 033310 (2023).

[40] A. Boudjemâa, Many-body and temperature effects in two-dimensional quantum droplets in Bose-Bose mixtures, Sci. Rep. **11**, 21765 (2021).

[41] M. A. Norcia, C. Politi, L. Klaus *et al.*, Two-dimensional supersolidity in a dipolar quantum gas, Nature (London) **596**, 357 (2021).

[42] T. Bland, E. Poli, C. Politi, L. Klaus, M. A. Norcia, F. Ferlaino, L. Santos, and R. N. Bisset, Two-dimensional supersolid

formation in dipolar condensates, Phys. Rev. Lett. **128**, 195302 (2022).

[43] G. Biagioni, N. Antolini, A. Alaña, M. Modugno, A. Fioretti, C. Gabbanini, L. Tanzi, and G. Modugno, Dimensional crossover in the superfluid-supersolid quantum phase transition, Phys. Rev. X **12**, 021019 (2022).

[44] H. Biss, L. Sobirey, N. Luick, M. Bohlen, J. J. Kinnunen, G. M. Bruun, T. Lompe, and H. Moritz, Excitation spectrum and superfluid gap of an ultracold fermi gas, Phys. Rev. Lett. **128**, 100401 (2022).

[45] W. Weimer, K. Morgener, V. P. Singh, J. Siegl, K. Hueck, N. Luick, L. Mathey, and H. Moritz, Critical velocity in the bec-bcs crossover, Phys. Rev. Lett. **114**, 095301 (2015).

[46] M.-O. Mewes, M. R. Andrews, N. J. van Druten, D. M. Kurn, D. S. Durfee, C. G. Townsend, and W. Ketterle, Collective excitations of a Bose-Einstein condensate in a magnetic trap, Phys. Rev. Lett. **77**, 988 (1996).

[47] D. S. Jin, J. R. Ensher, M. R. Matthews, C. E. Wieman, and E. A. Cornell, Collective excitations of a Bose-Einstein condensate in a dilute gas, Phys. Rev. Lett. **77**, 420 (1996).

[48] Y. Li, Z. Chen, Z. Luo, C. Huang, H. Tan, W. Pang, and B. A. Malomed, Two-dimensional vortex quantum droplets, Phys. Rev. A **98**, 063602 (2018).

[49] J. Wang, H. Hu, and X.-J. Liu, Thermal destabilization of self-bound ultradilute quantum droplets, New J. Phys. **22**, 103044 (2020).

[50] W. F. Ames, *Numerical Methods for Partial Differential Equations*, 3rd ed. (Academic, New York, 1992).

[51] J.-H. Zheng, B. Xiong, G. Juzeliūnas, and D.-W. Wang, Topological condensate in an interaction-induced gauge potential, Phys. Rev. A **92**, 013604 (2015).

[52] A. J. Leggett, Can a solid be "superfluid"? Phys. Rev. Lett. **25**, 1543 (1970).

[53] G. V. Chester, Speculations on Bose-Einstein condensation and quantum crystals, Phys. Rev. A **2**, 256 (1970).